IEEE Access
Multidisciplinary | Rapid Review | Open Access Journal

Received February 26, 2020, accepted March 18, 2020, date of publication April 22, 2020, date of current version May 21, 2020.

Digital Object Identifier 10.1109/ACCESS.2020.2989724

Comparison of Parameterization Methods for Real-Time Battery Simulation Used in Mechatronic Powertrain Test Benches

TASSILO SCHRÖDER, THOMAS GWOSCH, AND SVEN MATTHIESEN
IPEK–Institute of Product Engineering at Karlsruhe Institute of Technology (KIT), 76131 Karlsruhe, Germany
Corresponding author: Sven Matthiesen (sven.matthiesen@kit.edu)

This work was supported in part by the Federal Ministry for Economic Affairs and Energy under Grant 20Y1509B.

ABSTRACT This paper deals with the real-time simulation of a power tool battery pack on a mechatronic powertrain test bench. The ability of an easy-to-use model for quick and iterative test runs mainly depends on the effort of parameterization. For this purpose, an easily parameterizable battery model is required. The battery model used is based on the current state of research and simulates the battery's behavior with an adequate precision. The suggested parameterization allows building the model without the necessity of experimental investigation. Three different procedures for model parameterization were used and compared with the real battery behavior. In conclusion, this paper shows a good tradeoff between precision and an easy way to handle a battery model for testing mechatronic powertrains.

INDEX TERMS Batteries, modeling, parameter extraction, system analysis and design, system testing, mechanical engineering, mechanical systems, virtual prototyping, hardware-in-the-loop, mechatronic powertrain.

I. INTRODUCTION

Any machinery product development requires predictions as to the future product behavior. Therefore, an early validation of the product's overall system behavior is useful. In the context of powertrain validation testing with mechanical Hardware-in-the-Loop (HiL) test benches is quite established [1]–[10].

The use of mechanical test benches is also well-established in the validation of power tools. Especially in the case of battery-powered cordless power tools, the interactions between power source and mechanical powertrain are worth being paid attention to.

These interactions include the dependency of the driving speed on the battery voltage as well as the effects of dynamic torque loads on the battery's discharge behavior. Furthermore, the persistence of the power tool's performance is associated with the maximum current load of the battery. In this context, multiple use-cases and scenarios cause different battery requirements for power tools.

Hence, our first main question is how the power source influences the power tool's mechanical behavior in a mechanical HiL test bench.

The associate editor coordinating the review of this manuscript and approving it for publication was Wen-Sheng Zhao.

This raises the question whether a higher effort in the simulation of the power source enables a more precise analysis of the mechanical quantities in the early phases of the validation of power tools. The structural complexity of the model determines the effort required for parameterization.

To quantify the significance and the needed effort, we define a limit of accuracy, which the simulated power source has to pass. As the battery model should represent the electrical influence on the mechanical powertrain, we took the rotational speed as measured parameter. As a first approach, a limit of deviation of 5% between the rotational speed of the power tool with the simulated power source and the actual battery-powered power tool is acceptable.

Due to the small size of the power tools, the complete technical system fits into a mechanical HiL test bench. This circumstances leads to the requirement of a battery model that is real-time-capable. Furthermore, the battery model should be able to simulate the current dependence of the voltage, the thermal dependence, and the capacitive dependence.

For electric vehicles several battery models already exist [11]–[13]. These battery models are mostly incorporated in the vehicles' battery management system (BMS) [12]. Based on the model, the BMS ensures an efficient management of the battery's state of charge (SoC) and monitors the battery's state of health (SoH) through prediction of the battery's performance [12].

The literature reports three groups of battery models: electrochemical models, electrical models, and mathematical models. The accuracy and complexity of the different model types vary widely [9]. For the validation of battery packs for power tools the battery model must represent the behavior of the battery voltage and SoC for different dynamic current loads. Furthermore, the battery model's real-time capability is crucial for the integration into a HiL test bench. Besides, the model must be able to change the battery cell type and the circuit of the cells (connecting in series or parallel) easily. The uncomplicated modification of the battery setup, as regards circuit and cell type, is important because the model has to cover a wide range of applications. In the context of early validation in product development, the real-time capability and the easy parameterization of the model are more important than its precision and accuracy. The electrochemical models are not well suited for these requirements, because their structure is too detailed and complex for dynamic current loads and the prediction of SoC [14]. The electrical models are able to represent the electrical behavior of a battery pack [14]. The simplest of these models consists of an ideal voltage source with a resistor for the internal resistance of the battery cell. A more advanced version of this circuit is the RC model, in which a parallel RC circuit is in series to a resistor and an open-circuit voltage [14], [15]. Electrical circuit models are very accurate and are able to represent the dynamic electrical behavior of the battery [2], [3], [16]. In the context of HiL simulations, electrical models are also capable of simulating the thermal behavior of the battery cell [17]. However, the parameterization of these models needs experimental data from discharging tests of real battery cells [14], [16], [18]–[21]. In most cases, the simulation of the thermal properties of the battery cell also requires a high experimental effort or extensive modeling [22]–[24]. Therefore, a simple and easy changing of the battery cell type is not possible under these conditions. The mathematical models are not as accurate as the electrical circuit models [14], but they do not necessarily need as many experimental data from the battery cells as the electrical models [25]. This independence from experimental data is an advantage for the validation in the early phases of product development, since it offers the possibility of rapidly testing various battery cell types. Furthermore, the mathematical models are more likely to be real-time-capable, because they mainly consist of a differential equation [14].

Thus, as a first approach, a mathematical battery model was integrated into the HiL test bench for the validation of a cordless screwdriver.

Apart from the integration of the model into the HiL test bench, the model had to be parametrized. In this context, two aspects were crucial: the amount of needed parameters and the effort of determining these parameters. Especially, at the early stages of the product development process, the characteristics of the future product are mostly unknown. In addition, the variation of different components causes a high amount of testing iterations with different boundary conditions. Therefore, an easy and quick method of parameterization is quite practical. To keep the effort of parameterization as low as possible, the share of experimental parameter determination should be kept as low as possible.

Hence, we used different methods of parameterization that differ in the effort of parameter extraction. To compare the accuracies of the different parameterization methods with each other, we used a real battery pack as a benchmark. Therefore, we embedded the model and the battery pack in a test setup for cordless screwdrivers. In this setup the screwdriver operated with different torque loads, so that the impact of the model and the battery pack on the screwdriver's mechanical output parameters is measurable.

The paper therefore has the following order: Section II presents the methods and materials, which includes the mathematical model and its various parameterization methods,as well as the test setup, the test plan, and the data analysis. Section III presents the results of the various experiments, and Section IV discusses these results.

II. MATERIALS AND METHODS

A. MATHEMATICAL MODEL

As already mentioned in the introduction, a mathematical model is suitable for the rapid testing of different battery types and configurations. We used a mathematical model developed by Motapon *et al.* [26]. It is based on the work by Tremblay and Dessaint, who published a modified version of the Shepherd model in 2009 [25]. The model published by Tremblay and Dessaint enables a parameterization by the datasheet of the battery cell. Therefore, only three points on the manufacturers discharge curve are required [25]. Indeed, the battery model by Tremblay and Dessaint does not consider the thermal behavior of the battery. This disadvantage is considered in the model by Motapon *et al.* [26]. Accordingly, it is an extended version of the model by Tremblay and Dessaint, as it adds the thermal behavior of the battery. In this context, the model by Motapon *et al.* fulfills our requirements, as it is a suitable tradeoff between parameterizability and precision. The Montapon battery model considers the thermal impact on the batteries' charge and discharge behavior. For the parameterization of this model, two discharge curves, at different temperatures from the manufacturers datasheet, are required. Furthermore, two of the parameters are determined using a simple thermal performance test [26]. Overall, this latest battery model is a good tradeoff between an accurate simulation and an easy parameterization and configuration of different battery cell tvpes. The central term of the model is the modified Shepherd equation, which is as follows.

$$V_{Batt} = E_0 - K\left(\frac{Q}{Q-it}\right)it - Ri - K\left(\frac{Q}{Q-it}\right)i^* + A\exp\left(-B\cdot\frac{it}{Q}\right) - Cit \quad (1)$$

According to [26], the equation consists of the battery thermodynamic voltage E_0, the polarization constant K, the

battery capacity Q, and the internal resistance R. The exponential term at the end of the equation describes the

voltage drop at the beginning of the discharge. The variable i is the discharge current of the battery cell, thus it is the integration of current over time and i^* is the current filtered by a low-pass filter. As already mentioned in [25], the parameters A, B, and C can be extracted directly from the discharge curve of the datasheet of the battery cell. The parameters E_0, K, R, and Q depend on thermal influences. In this context, the following equations describe the dependence between the temperature of the battery cell and the parameters.

$$E_0(T) = E_{0|T_{ref}} + \frac{\delta E}{\delta T}\left(T - T_{ref}\right) \tag{2}$$

$$K(T) = K_{|T_{ref}} \cdot \exp\left(\alpha\left(\frac{1}{T} - \frac{1}{T_{ref}}\right)\right) \tag{3}$$

$$R(T) = R_{|T_{ref}} \cdot \exp\left(\beta\left(\frac{1}{T} - \frac{1}{T_{ref}}\right)\right) \tag{4}$$

$$Q(T_a) = Q_{|T_{ref}} + \frac{\Delta Q}{\Delta T}\left(T_a - T_{ref}\right) \tag{5}$$

In Equations (2) to (5), T is the current temperature of the battery cell, while T_{ref} is the reference temperature, at which cell discharging starts. The current temperature T depends on the discharge current and will be calculated by the model. The structure of the battery cell model, therefore, is as follows.

As shown in Figure 1, the model contains three loops, which all lead to the calculation of the power loss. In this model the power loss causes the thermal strain of the battery cell, hence summarizing the internal losses of the ohmic resistances inside the battery cells. The following equation

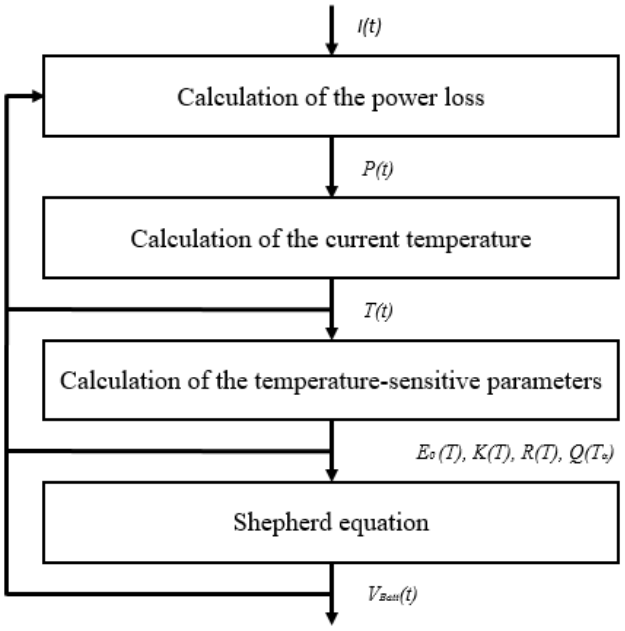

FIGURE 1. Schematic structure of the model according to [26].

calculates this power loss.

$$P_{loss} = \left(E_0(T) - V_{batt}(T)\right) i + \frac{\delta E}{\delta T} iT \tag{6}$$

The first term of the equation includes the losses of the polarization and the internal resistance. These losses depend on the current voltage of the battery V_{batt} and the battery thermodynamics voltage E_0 [26]. Due to the change of V_{batt} and E_0 during the discharging of the battery cell, both factors have to be calculated in a loop. The second term considers the reversible losses, which were caused by the electrochemical reaction inside the battery cell [26]. To this reaction, the cell temperature is relevant, which is the reason why the current temperature is also calculated in a loop. For the equation of the current temperature a simplification will be made. This simplification assumes that the temperature of the whole battery pack is equivalent to the surface temperature of the hottest cell [26]. Therefore, the temperature of the battery pack can be derived from the power loss as follows [26].

$$T(t) = \mathcal{L}^{-1}\left(\frac{1}{1 + s \cdot t_c} \cdot \left(R_{th} \cdot P_{loss}(s) + T_a(s)\right)\right) \tag{7}$$

As is shown in (7), the temperature is the inverse Laplace transform of the power loss $P_{loss}(s)$ and the ambient air temperature $T_a(s)$. The equation also contains two factors: on the one hand, the thermal resistance R_{th}, and on the other hand, the thermal time constant t_c. According to [26], both parameters have to be determined experimentally. The next part of the model calculates the temperature-sensitive parameters of the Shepherd equation by using Equations (2) to (5). For solving these equations, eight parameters $x = (\boldsymbol{E_{0|T_{ref}}}|\boldsymbol{K}_{|T_{ref}}|\boldsymbol{R}_{|T_{ref}}|\boldsymbol{Q}_{|T_{ref}}|\frac{\delta E}{\delta T}|\boldsymbol{\alpha}|\boldsymbol{\beta}|\frac{\Delta Q}{\Delta T})$ are required. These parameters can be extracted from the discharge curves of the battery cell [25], [26]. Two discharge curves at different temperatures are needed. On these curves, the voltage and the charge of the battery cell have to be determined at eight significant spots [26]. By using the values of the battery voltage at these spots, it is possible to create a system of equations. The nonlinear least squares algorithm *isqnonlin* of the *Matlab optimization toolbox* is used for solving these equations [26]. The parameters A, B, and C from Equation (1) can be calculated directly from the discharge curve as shown in [25] and [26]. In the mathematical model introduced, the main part of the parameterization can be done by extracting data from the datasheet of the battery cell. Only the thermal resistance R_{th} and the thermal time constant t_c have to be identified experimentally. It can be seen that the structure of the model is very similar to [17], although it is based on a fully mathematical model of the battery cell.

B. PARAMETERIZATION METHODS

As already mentioned in the introduction, the ability of an easy-to-use model to carry out quick and iterating test runs mainly depends on the effort of parameterization. Hence, the following chapter suggests three different methods of

TABLE 1. Parameters of the battery model.

Symbol	Parameter name	Unit
T_1	Temperature for discharge curve 1	K
T_2	Temperature for discharge curve 2	K
I	Discharge current	A
R_{th}	Thermal resistance	K/W
t_c	Thermal time constant	s

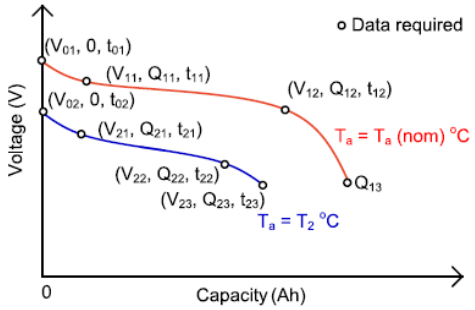

FIGURE 2. Two discharge curves with the significant points of operation for the parameterization of the battery model, taken from [26].

parameterization to create three sets of parameters. Due to the structure of the model, each parameterization method requires two discharge curves at different ambient air temperatures. On each curve, the values of the voltage and load were extracted at four significant instances of time [26]. The significant points of operation are shown exemplarily in Figure 2, which is taken from [26]. In addition, Table 1 sums up all parameters, that are needed for the parameterization of the battery model.

The values of voltage, load, and temperature from the discharge curve enabled calculation of the parameters $x = (E_{0|T_{ref}}|K_{|T_{ref}}|R_{|T_{ref}}|Q_{|T_{ref}}|\frac{\delta E}{\delta T}|\alpha|\beta|\frac{\Delta Q}{\Delta T})$ by using a least squares algorithm [26]. With reference to [26], the temperature at the different significant points can be calculated by using Equations (8) to (13), as shown at the bottom of this page.

C. FIRST METHOD OF PARAMETERIZATION

The first parameterization method uses the approach, already suggested in [26]. Accordingly, the created parameter set is mainly based on the datasheet of the battery cell. Therefore, we take two discharge curves at different ambient air temperatures from the datasheet. For the experimental determination of R_{th}, and t_c, the suggested experiment from [26]. were carried out. Therefore, a thermocouple type J was integrated in a Bosch lithium-ion (Li-Ion) battery pack with a capacity of 2 Ah and a nominal voltage of 18 V. The battery pack contains five Panasonic format-18650 cylindrical cells [27]. According to [26], a position between the battery cells was chosen for placement of the thermal sensor. Furthermore, the suggested procedure for charging and discharging was used for the calculation of R_{th} and t_c. The procedure suggested in [26] includes charging and discharging of the battery pack with a constant current load until the temperature difference of 10 K to the initial temperature is reached. With reference to [26], we calculated both parameters with the measured data and by using Equations (14) to (18) [26].

$$t_c = t_2 - t_1 \tag{14}$$

$$T_{i2} = (T_{i1} - T_a)e^{-1} + T_a \tag{15}$$

$$P_{l2} = V_2 \cdot i_1 \left(\frac{1}{\zeta} - 1\right) \tag{16}$$

$$\zeta = \frac{V_1}{V_2} \tag{17}$$

$$R_{th} = \frac{T_{i1} - T_a \cdot \left[1 - e^{\left(-\frac{t_3}{t_c}\right)}\right] - T_{i0} \cdot e^{\left(-\frac{t_3}{t_c}\right)}}{P_{l2} \cdot \left[1 - e^{\left(-\frac{t_3}{t_c}\right)}\right]} \tag{18}$$

$$T(t_{01}) = T_1 \tag{8}$$

$$T(t_{11}) = \frac{\left[\left(E_0 - \frac{\partial E}{\partial T} \cdot T\,(t_{01}) - V_{11}\right) \cdot i \cdot R_{th} + T(t_{01})\right] \cdot \left[1 - exp\left(-\frac{t_{11}}{t_c}\right) \cdot (1 - T(t_{01}))\right]}{1 - 2 \cdot \left[1 - exp\left(-\frac{t_{11}}{t_c}\right) \cdot \frac{\partial E}{\partial T} \cdot i \cdot R_{th}\right]} \tag{9}$$

$$T(t_{12}) = \frac{\left[\left(E_0 - \frac{\partial E}{\partial T} \cdot T\,(t_{01}) - V_{12}\right) \cdot i \cdot R_{th} + T(t_{01})\right] \cdot \left[1 - exp\left(-\frac{t_{12}}{t_c}\right) \cdot (1 - T(t_{01}))\right]}{1 - 2 \cdot \left[1 - exp\left(-\frac{t_{12}}{t_c}\right) \cdot \frac{\partial E}{\partial T} \cdot i \cdot R_{th}\right]} \tag{10}$$

$$T(t_{02}) = T_2 \tag{11}$$

$$T(t_{21}) = \frac{\left[\left(E_0 - \frac{\partial E}{\partial T} \cdot T\,(t_{01}) - V_{21}\right) \cdot i \cdot R_{th} + T(t_{02})\right] \cdot \left[1 - exp\left(-\frac{t_{21}}{t_c}\right) \cdot (1 - T(t_{02}))\right]}{1 - 2 \cdot \left[1 - exp\left(-\frac{t_{21}}{t_c}\right) \cdot \frac{\partial E}{\partial T} \cdot i \cdot R_{th}\right]} \tag{12}$$

$$T(t_{22}) = \frac{\left[\left(E_0 - \frac{\partial E}{\partial T} \cdot T\,(t_{02}) - V_{22}\right) \cdot i \cdot R_{th} + T(t_{02})\right] \cdot \left[1 - exp\left(-\frac{t_{22}}{t_c}\right) \cdot (1 - T(t_{02}))\right]}{1 - 2 \cdot \left[1 - exp\left(-\frac{t_{22}}{t_c}\right) \cdot \frac{\partial E}{\partial T} \cdot i \cdot R_{th}\right]} \tag{13}$$

The values of R_{th} and t_c calculated based on the measured data are shown in Table 2.

TABLE 2. Values for the thermal resistance and the themal time constant according to the experimental results.

Symbol	Parameter name	Unit	Value
R_{th}	Thermal resistance	K/W	1.46
t_c	Thermal time constant	s	2066

Table 3 shows the values of the voltage and the capacities at the discrete points we extracted from the discharge curve of the datasheet [27] according to [26].

TABLE 3. Values for the voltage and the capacities extracted from the discharge curve [19].

No.	Description	Unit	Value
1	Vector of the voltage values at the discrete points $[V_{01},V_{11},V_{12},V_{02},V_{21},V_{22}]$	V	[4.16, 4.09, 3.35, 4.05, 3.98, 3.32]
2	Vector of the capacities values at the discrete points $[Q_{01},Q_{11},Q_{12},Q_{02},Q_{21},Q_{22}]$	As	[0, 92, 6624, 0, 168.2, 5688]

D. SECOND METHOD OF PARAMETERIZATION

The second parameterization method extracts the values of the voltage and the current load from the datasheet as well. However, for determination of R_{th}, and t_c, we used the values calculated from the experiments in [26]. With this procedure, we want to check whether the values of the thermal resistance and the thermal time constant have an influence on the output values of the HiL test bench. If the thermal time constant and thermal resistance are negligible, then the parameterization of the model is based exclusively on the data sheet. In this context, a physical battery cell for parameterization is no longer necessary. Thus, a larger variation of different cells can be simulated faster and more easily. Table 4 shows the referred values of the thermal resistance and the thermal time constant from [26].

E. THIRD METHOD OF PARAMETERIZATION

Our third parameterization method consists in a full experimental parameterization of the battery model. In this context, ''full, experimental parameterization'' means a parameterization that is fully based on the experimental measured data of a discharged battery. Instead of taking the significant points of the discharge curve (shown in Figure 2) from a datasheet, we created two discharge curves on our own by discharging the real battery pack in a climate chamber. Therefore, the Bosch battery pack with the type-J thermocouple was put in a thermally isolated box and was discharged with a

TABLE 4. Literarture based values for the thermal resistance and the themal time constant according to [18].

Symbol	Parameter name	Unit	Value
R_{th}	Thermal resistance	K/W	0.629
t_c	Thermal time constant	s	4880

current of 2 A at temperatures of 273 K and 293 K. For better comparability, the temperature levels for discharge, and the discharge current, were chosen to be the same as those in the datasheet.

For cooling of the battery pack, a heat exchanger provided by Wätas Wärmetauscher Sachsen GmbH was connected to a Unistat® 425 chiller made available by Huber Kältemaschinenbau AG. Furthermore, the battery pack was connected to an electronic load (EL 9000 B 2Q by EPS Stromversorgung GmbH), the load discharged the pack with a constant current, and recorded the battery pack's voltage over time. The values of voltage (V), load (Q), and temperature (T) at the specific points (Figure 2) were manually selected by using the Matlab function input (g). With this selection and the parameters of Table 2, one set of parameters was created. The set uses the recorded temperature values for determining the temperature vectors $[T_{01}, T_{11}, T_{12}, T_{02}, T_{21}, T_{22}]$. Table 5 shows the measured voltages, capacitances and temperatures at the discrete points of the recorded discharge curve. Note that these are the values for the entire battery pack. Hence, for the voltage values, five battery cells were connected in series.

TABLE 5. Values for the voltage and the capacities extracted from the discharge curve [19].

No.	Description	Unit	Value
1	Vector of the voltage values at the discrete points $[V_{01},V_{11},V_{12},V_{02},V_{21},V_{22}$	V	[20.87, 20.27, 16.69, 20.93 19.44 16.43]
2	Vector of the capacities values at the discrete points $[Q_{01},Q_{11},Q_{12},Q_{02},Q_{21},Q_{22}]$	As	[0, 71.56, 5415.46, 0, 124.03, 4695.26]
3	Vector of the temperature values at the discrete points $[T_{01}, T_{11}, T_{12}, T_{02}, T_{21}, T_{22}]$	K	[293.24, 293.88, 298.1, 273.5, 273.76, 278.59]

In summary, we compared the performance of these three different parameter sets with each other. Table 6 lists the different types of parameter extractions.

F. TEST SETUP

Figure 3 shows the test setup. Based on a Simulink implementation, we integrated the battery model in the control system of the test bench. An ADwin Pro-II system provides the real-time control. The test bench control is connected to

TABLE 6. Different precedures for the parametrization of the battery model.

No.	Description	Time and effort of parametrization
1	Calculating the model's parameters from the battery cell's datasheet, determining R_{th} and t_c experimentally as suggested in [18] .suggested	medium
2	Calculating the model's parameters from the battery cell's datasheet, determining R_{th} and t_c by using literature- based values from [18]	low
3	Calculating the model's parameters from an experimentally determined discharge curve of a battery pack, calculating the temperature at the significant points out of the timestamps and the significant voltage values by using the Equations 11 to 15, determining R_{th} and t_c experimentally as suggested in [18]. suggested	high

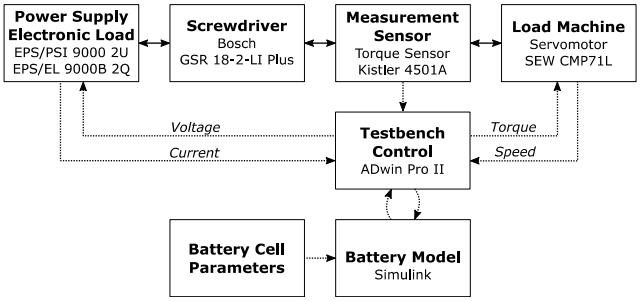

FIGURE 3. Experimental test setup on the test bench (schematically).

the power supply hardware. The controllable power supply is the power stage of the battery simulator. The electronic load enables a two-quadrant operation. Hence, the power supply and electronic load are connected and are in the master-slave mode. The power supply is connected to the electronics of the cordless screwdriver. Figure 4 shows a photography of the mechanical part of the test rig with the screwdriver. During the test setup, we mounted a torque sensor on the drill chuck and connected it mechanically to the loading machine. The test bench control controls the screwdriver via a trigger signal.

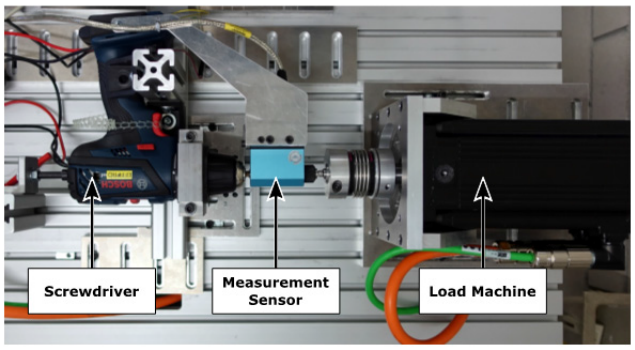

FIGURE 4. Mechanical part of the test bench with cordless screwdriver [28].

The measurement variables are electric voltage and current, torque, and speed at the mechanical output shaft of the screwdriver.

For the tests a mechanical load profile is used, and the trigger position is a given value. The parameterization of the battery model is carried out by the cell datasheet and the mentioned calculations (compare Section II). The parameters used can be taken from Table 2 and Table 6 [12].

G. EXPERIMENTAL-APPROACH METHODS

To answer the two main questions introduced, namely firstly, as to whether the battery's influence on the power tool's mechanical behavior is as significant as requiring simulation of the battery pack in the HiL test bench, and secondly, as to how much effort it takes to simulate the battery influence on the mechanical powertrain, we did the following experiments. Therefore, we used two different test setups. Figure 5 shows a schematic overview of these test setups. In test setup 1, we connected the Bosch battery pack and the power supply with the different parametrized models to an electronic load. The aim of analysis was to review whether the different parametrized models generally behave in a way comparable to that of the battery pack. For this purpose, a static current load of 10 A and square-wave current with an amplitude of 10 A were applied to the different power sources by the electronic load. As comparative value, we measured the delivered voltage of the different power sources.

After these purely electrical experiments, we used test setup 2 to analyze the mechanical-electrical interaction between the different power sources and the cordless screwdriver. We attached the power supply to the battery model and the battery pack to the cordless screwdriver of the described HiL test bench. In order to generate a current load at the power connection of the cordless screwdriver, we connected the device to an SEW CMP71L load machine and applied a torque load.

We applied the torque load to the screwdriver in two different ways. In this context, the experimental approach provided a load duration of 20 s at each torque level. This load duration was repeated three times in a row without recharging the battery pack or reloading the model. Before we introduced the next torque level, we recharged the battery pack or set the SoC of the battery model to 100% again.

Besides dealing with the different battery models and the battery pack, we repeated the whole procedure with a constant voltage source. The constant voltage source is a reference for verifying the influence of the battery's behavior on the mechanical output parameter during hardware-in-the-loop testing of the power tools. Hence, we run the power source at constant values of 18 V and 20 V. The value of 18 V equates to the nominal voltage of the battery pack, the value of 20 V was measured at the pins of the fully charged battery pack.

Finally, we evaluated the different parameterized battery models under the conditions of a real screwing test and real drilling test. With this experimental approach, the models' performance in the context of real applications was tested.

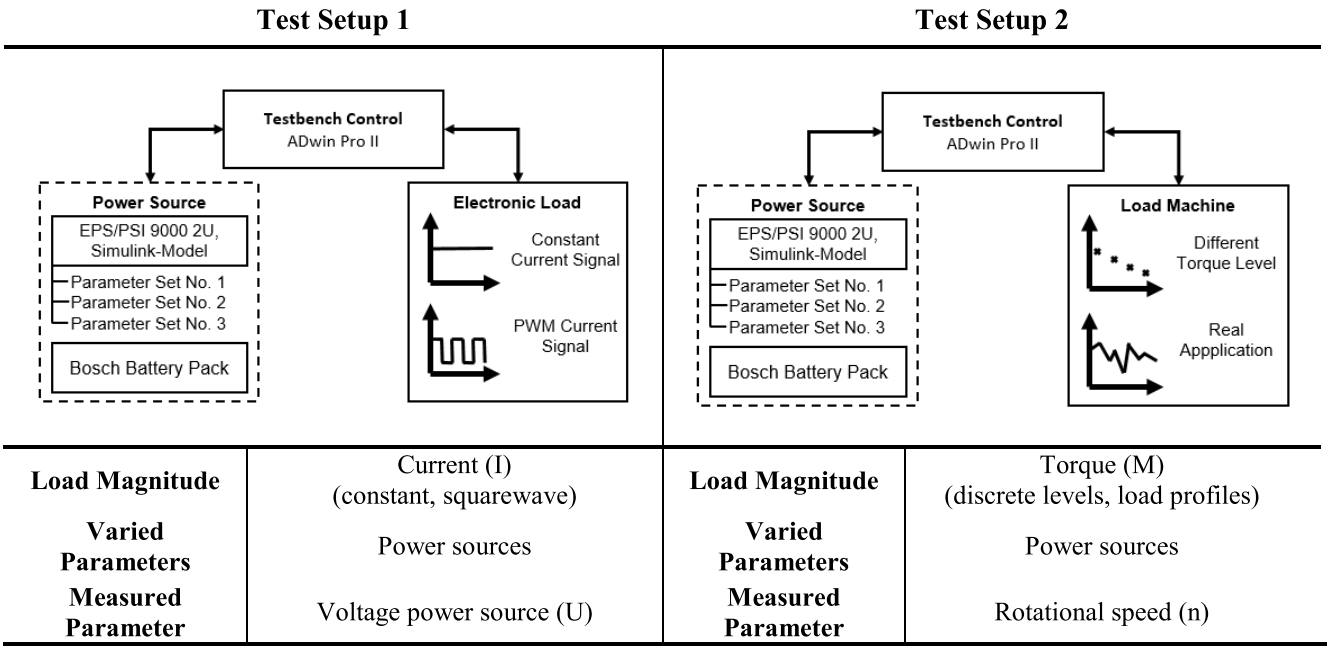

FIGURE 5. Schematic representation of the experimental design.

We compared the accuracy of the different parametrized models in the validation process of a HiL test bench. For this purpose, the cordless screwdriver of the HiL test bench was equipped with a rotational speed and a torque sensor. We then carried out several screwing and drilling tests in a wooden beam while recording the speed and the profiled torque load. For the drilling experiments, we drilled with a drill diameter of 6 mm into a wooden beam. For screwing, we screwed 5×60 mm wood screws into a wooden beam.

The gained courses of torque load were transferred to the load machine of the HiL test bench. Thus, in the following experiment, the HiL test bench loaded the cordless screwdriver with these torque courses, while it was powered by the different parameterized battery models. As a measured variable, we compared the rotational speed with the real screwing and drilling tests of the cordless screwdriver.

III. RESULTS

The first part of the results chapter shows the plots of test setup 1. As you can see in Figure 6, an electronic load discharged the different parameterized battery models and the real battery. In this test setup, we used a constant and a square-wave current load of 10 A for discharging. The corresponding voltage curves are plotted in Figures 6 and 7.

In Figure 6, almost over the entire capacity range, the discharge curves of all three parameter sets are above the discharge curve of the original battery run within a maximum offset of 2 V. All of the three different parameterized models simulate the voltage drop at the beginning of the discharge. However, it is much more pronounced in the real battery than in the battery model. When comparing all of the three parameter sets, the curve of the model parametrized with parameter

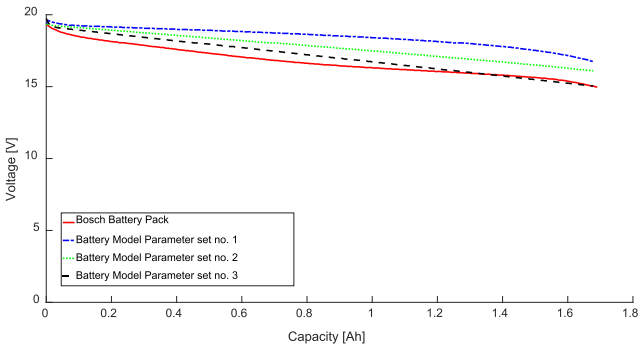

FIGURE 6. Discharging of the battery pack and the battery model with a constant current load of 10 A.

set no. 3 has the lowest offset to the discharge curve of the real battery. However, the course of the discharge curve of parameter set no. 3 does not match with the course of the real discharge curve. While the discharge curve of the real battery has a hyperbolic form, the voltage in the simulation with parameter set no. 3 decreases mainly linearly. In contrast, the discharge curve of parameter set no. 1 is also slightly hyperbolic. Thus, the course of parameter set no. 1 has the highest similarity to the real discharge curve. Nevertheless, the curve of parameter set no. 1 has the largest offset for discharging the battery pack. The course of the discharge curve of parameter set no. 2 is very similar to the course of the discharge curve of parameter set no. 3. After the voltage drop at the beginning, both curves show a largely linear behavior. However, the gradient of parameter set no. 2 is larger than the gradient of parameter set no. 3. The larger gradient of the curve of parameter set no. 2 leads to a larger offset from the real battery pack. The offset of the discharge curve of

parameter set no. 2 is approx. 1.2 V, which is smaller than the offset of the discharge curve of parameter set no. 1.

In Figure 7, the load magnitude is changed to a square-wave current load. The course curve of parameter sets no. 1, no. 2 and no. 3 in Figure 7 is comparable to the discharge with a constant current load in Figure 6. Both the battery model and the real battery pack react in a similar way to the influence of the square-wave current load. The same amplitudes of the real battery pack and the different parameterized models also reflect this correlation. In this context, the amplitude of the discharge curve of parameter set no. 2 represents an exception, because it decreases with time.

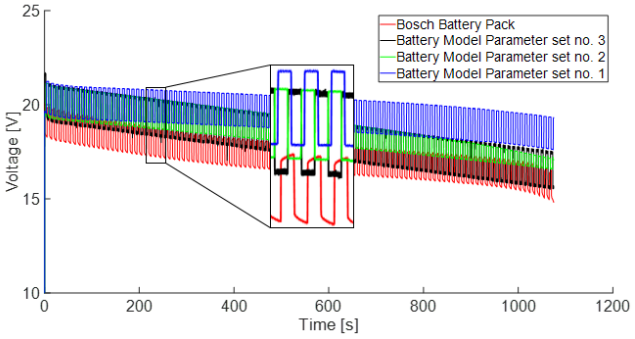

FIGURE 7. Discharging curves of the battery pack and the battery model with a square waved, time-shifted current load of 10 A.

The frequencies of the discharge voltage curves also correspond with the frequency of the current load. The detail view of the plot displays a phase displacement between the different discharge curves. Besides this phase displacement, the detail view also shows differences in the amplitudes of the square-wave voltage signals. While the amplitudes of parameter sets no. 1 and no. 2 are flat-topped, the amplitude of parameter set no. 3 has a noisy characteristics. The peaks of the real battery pack have a chamfered characteristics.

In the test setup, the battery models and the battery pack were connected to an electric screwdriver, which was mechanically connected with an adjustable load machine as is shown in Figure 5. At first, this electric screwdriver was loaded with different torque levels for each of the different power sources.

Hence, Figure 8, Figure 9, and Table 7 show the values and plots for the rotational speed among different torque levels.

TABLE 7. Gradient of the linear Regression for different power sources.

Power Source	Gradient [rpm/Nm]
Bosch Battery Pack	-21.7
Battery Model Parameter set no. 1	-24.2
Battery Model Parameter set no. 2	-11.0
Battery Model Parameter set no. 3	-23.5
Constant Voltage 18V	-14.7
Constant Voltage 20V	-15.8

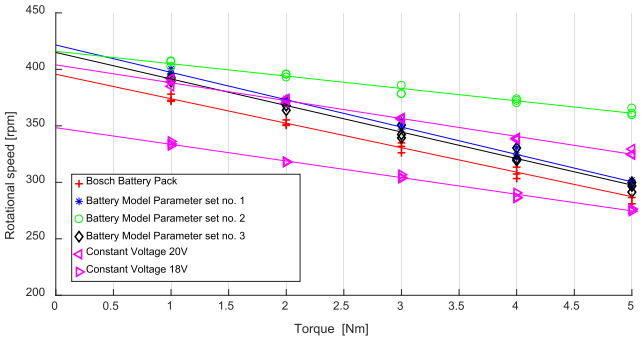

FIGURE 8. Averaged rotational speed over different torque levels with linear regression lines.

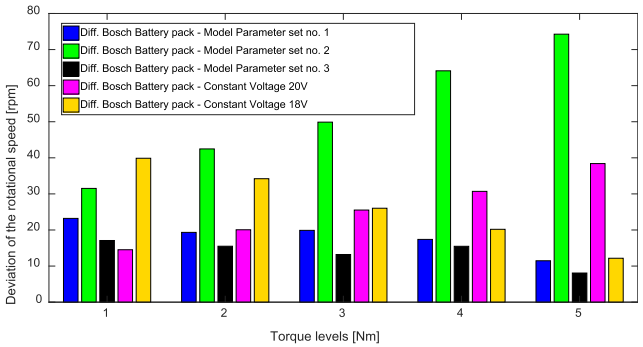

FIGURE 9. Deviation between the different power sources and the real battery pack.

The plots in Figure 8 show the average rotational speeds of the different power source parameterizations for different torque levels. A linear regression line is plotted through these discrete working points. In addition, Table 7 lists the gradients of these regression lines. Furthermore, Figure 9 shows the percentage deviation of the rotational speed between the different power sources and the actual battery pack.

The regression lines in Figure 8 show a large variation between the different parameterization methods, the real battery pack, and the constant voltage sources. The gradients of the battery pack and the model values of the parameter sets no. 1 and no. 3 vary in the range between -20 rpm/Nm and -25 rpm/Nm, as shown in Table 7. In comparison, the gradient values of the constant voltage sources are around -15 rpm/Nm. The model parameterized with parameter set no. 2 deviates most from the real battery pack. The deviation of the regression line of parameter set no. 2 from the regression line of the real battery pack is even greater than the deviation of the constant voltage sources. In this context, Figure 8 corresponds to the gradient value of parameter set no. 2 in Table 7, which is around 11 rpm/Nm. The regression line's gradient of parameter set no. 2 is consequently around half as large as the gradient of the real battery pack. As a consequence, the deviation between the model parametrized by parameter set no. 2 and the real battery pack rises over the rising torque levels.

The bar chart in Figure 9 confirms the results shown in Figure 8. The chart shows a rising deviation between the rotational speed values of the real battery pack and the rotational speed values of the model parametrized with parameter set no. 2. This deviation reaches its peak at a torque level of 5 Nm within a percentage deviation of about 25%.

In the second part of the experiments, which carried out with test setup 2, we tested the performance of the different parameterization methods under the condition of a real application.

Therefore, we changed the torque load of the load machine from the discrete torque levels to the torque characteristics of a real application with a dynamic load profile.

The chosen applications were drilling and screwing with a cordless screwdriver. Figure 10 shows the plots of the rotational speeds of the different power sources for the drilling application. Figure 11 shows the plots of the rotational speeds of the different power sources for the screwing application with the cordless screwdriver.

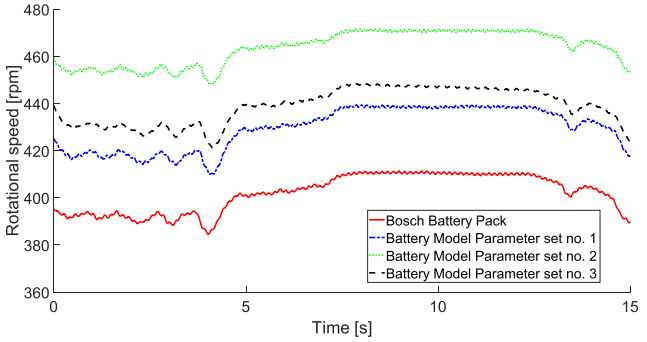

FIGURE 10. Cutout of the rotational speed of a screwdriver for a drilling application with the Bosch battery pack and battery model with parameter sets no. 1 to 3.

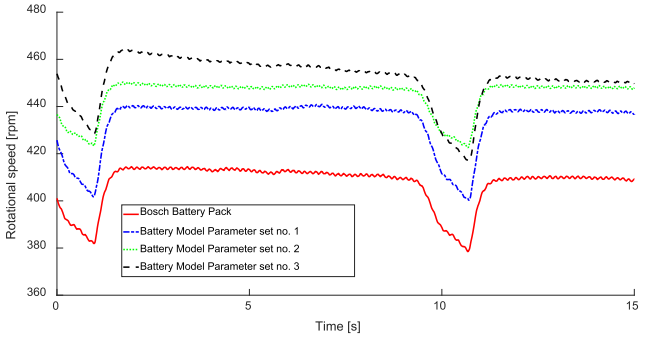

FIGURE 11. Cutout of the rotational speed of a screwdriver for screwing application with the Bosch battery pack and battery model with parameter sets no. 1 to 3.

While the drilling process takes about 10 seconds, the screwing process takes much less time. In the case of screwing, the impact of the torque load on the rotational speed is clearly visible and is separated by defined sequences. In the case of drilling, the impact is imprecise and not as distinct, since the curve is more discontinuous. In addition, the speeds for drilling and screwing are in a similar range. In both cases, a clear offset between the original application and the mapping on the test bench is visible. This offset is positive for all parameterization methods. Thus the rotational speeds of the different parameterized models are generally greater than in the real application. Furthermore, the courses of the rotational curves of the original application and the mapping on the test bench are similar for all parametrization methods.

Concerning the drilling, the results shown in Figure 10 are comparable to those shown in Figure 8. While the curve of parameter set no. 2 has the greatest offset, the curves of parameter sets no. 1 and 3 are very close to each other. In addition, as shown in Figure 8, the curve of parameter set no. 3 goes beyond that of parameter set no. 1.

In the screwing application, the curves of the different parameterized models are closer together than in the drilling application. Figure 11 also shows a slight overlap of the speed curves for parameter set no. 2 and parameter set no. 3. Furthermore, the rotational speed curve of parameter set no. 2 is below the curve of parameter set no. 3.

IV. DISCUSSION

Based on the initial questions, the results of the experiments carried out are discussed below. The initial questions are how the power source influences the power tool's mechanical behavior at a mechanical HiL test bench and whether, in the early phases of the validation of power tools, a higher effort in the simulation of the power source enables a more precise analysis of the mechanical quantities.

To answer these questions, we first concentrate on the results of test setup 1, then compare and analyze the accuracy and basic suitability of the different parameterization methods for mechanical HiL test bench applications of test setup 2. Figures 6 and 7 show the model's ability to react to static and dynamic current loads in a similar way as a battery pack. However, the different parametrized models differ widely in the adaptation between the curve of the models and the curve of the battery pack. From this, we can conclude that the parameterization methods have a large influence on the discharge characteristics of the battery model, even if the parameterization is based on the same cell type. The model used is also less accurate than the already established battery models [14], [15], [26]. As already mentioned, a mathematical battery model was used for the experiments. Generally, mathematical models are less accurate than electrical models [14]. Thus, the inaccuracy of the employed model is not unusual compared to that of electrical experiments [14].

In this context, it has to be mentioned that the fitting of our results is also less accurate than the results found by Motapon *et al.* in [26]. This observation is unexpected, especially in the case of parameter set no. 1, which was extracted from the datasheet and the experimental data as suggested in [26]. A possible explanation for this deviation is that the simulation does not consider aging effects and the state of health (SoH). The battery pack we used for testing has

been used several times before, so the SoH of the cells has already suffered from aging effects. In contrast, the reported discharge curve on the datasheet is recorded with an optimal battery cell under ideal conditions. Since the SoH of the real battery cell is not mentioned in [26], it can be presumed that this battery cell was rarely discharged before verification of the model. This presumption would explain the worse fitting of our discharge curve compared to [26] in Figure 6. The fact that the plot of parameter set no. 3 in Figure 6 only has a small offset to the real battery pack supports this hypothesis. All parameters of set no. 3 were taken from the measurement of the real battery. Hence, these extracted parameters include the aging effects the real battery pack had suffered from.

With regards to parameter set no. 2, Figure 6 shows that its plot runs below that of parameter set no. 1. Since the only difference between parameter set no. 1 and parameter set no. 2 is the values of R_{th} and t_c, this difference must be caused by these two parameters. In consequence, the lower values of R_{th} and t_c must cause this deviation.

The observations from Figure 6 are also visible in Figure 7, hence the deviation in the accuracy of the models is slightly the same as in Figure 6. Especially since the different discharge curves have the same order and the same offset that they already had in the discharging with the constant current load.

Furthermore, Figure 7 shows the ability of the battery model to handle a dynamic current load. The model's response is not changed by an alternating load, the similar voltage amplitudes of the model and the battery pack show that both systems respond in a comparable way. Only to parameter set no. 2 this statement does not apply. As can be seen in Figure 7 the amplitude of the model parameterized by parameter set no. 2 decreases with time. Since the testing conditions and the other parameters are the same as in the experiments with parameter set no. 1, it can be concluded that the different values for R_{th} and t_c are responsible for this decrease.

The phase shift, which is visible in the detail view of Figure 7, is caused by the phase shift of the current load in the experiment.

In summary, the results of the experiments of test setup 1 lead to several statements. The mathematical model is limited in its accuracy under the condition of simulating the discharging of a real battery pack. This limitation affects all parameterization methods in general, since the SoH is not simulated and the mathematical models as such are limited in their accuracy [14]. Regarding the different parameterization methods, we obtain the following statements. With regard to the qualitative course of the discharge curve, parameter set 1 is the most suitable, as it behaves most like a real battery in terms of discharge behavior. However, the great offset causes a lack of accuracy. The changing of parameters R_{th} and t_c has a huge impact on the performance of the model, even without the simulation of extreme thermal conditions. The higher effort of experimental data extraction for parameter set no. 3 does not lead to a more accurate simulation than expected. Although the offset between the real discharge curve and the curve of parameter set no. 3 is the smallest, the discharge behavior does not fit with the discharge behavior of the battery pack.

Regarding the results of test setup 2, we will discuss the electrical-mechanical interaction on the mechanical HiL test bench.

The plots in Figure 8 and the corresponding gradients in Table 7 give a first impression of the models' performance at discrete working points. The analysis of the recorded results (see Figure 8) reveals that the slope of the linear regression line indicates the battery to have a significant influence on the mechanical output parameters. This influence is caused by the current dependence of the battery. Therefore, the torque not only affects the motor of the power tool, but also influences the battery by the current or torque load. This influence is also visible in the different gradients of the linear regression lines as shown in Table 7. In order to make a quantitative statement, we consider the percentage deviations of the rotational speed in Figure 8. Therefore, as a first approach, we have introduced a limit of 5% acceptable deviation between the model and the real battery pack. Figure 8 as well as Figure 9 point out that the percentage deviation parameter set no. 2 is far beyond this limit and performs for high torque levels even worse than the static voltage sources. In addition, the percentage deviation of the constant voltage sources distorts the rotational speed of the screwdriver. The error of the 20 V source increases beyond the acceptable limit of 5% within the rise of torque, while the 18 V source's error increases beyond 5% for the lower torque levels. With regard to the introduced definition, the distortion of the rotational speed is beyond the acceptable limit.

Based on these two observations, two conclusions can be made. The first is that the absent current respectively torque dependency of the constant voltage source has a distorting influence on the system's mechanical behavior. Consequently, the plots of the constant voltage source actually represent the motor characteristics of the cordless screwdriver's PMDC motor. Due to the gradient of the regression lines, any constant voltage source cannot map the cordless screwdriver's behavior correctly since the motor characteristics of a PMDC motor show same rate of change for different levels of voltage. Hence, the results of the experimental investigation lead to the conclusion that the power source has an influence on the mechanical output parameters of the HiL cordless screwdriver test bench.

Secondly, the massive distortion of the rotational speed, which the cordless screwdriver experiences through the parameterization with parameter set no. 2 shows that this parameterization method is not suitable for parametrization.

According to Figure 3 and under the condition of a 5% deviation limit, only parameter set no. 3 is suitable for the parameterization of the model. In view of the effort required to extract the experimental data for parameter set no. 3, it is questionable whether it is useful for a slightly better result on the test bench.

If we consider the results from Figure 10 and Figure 11, this conclusion becomes even more debatable. In Figure 10, the curve of parameter set no. 3 runs beyond that of parameter set no. 1. This result does not correspond with the results from Figure 8. Nevertheless, the ratio of the offset of the curves of the different parameterized models to each other and to the real battery pack is comparable with the results shown in Figure 8. In both figures, for example, the curve of parameter set no. 2 is far above that of the battery pack. Apart from the interchanged order of the offset, the curves of parameter sets no. 1 and no. 3 are also as close to each other as in Figure 8. From this observation we conclude that the load type has no influence on the performance of the model as such. As a result, the reversed order of parameter sets 1 and 3 with respect to the offset from the speed curve of the battery pack is due to the parameterization method of parameter set no. 3. Figure 11 supports this conclusion. In Figure 11, the rotational speed of parameter set no. 3 has the largest offset to the rotational speed curve of the screwing application. This inconsistence in the drilling and the screwing application worsened the accuracy of parameter set no. 3.

Regarding all experiments we have made with test setup 2, the model parameterized with parameter set no. 1 has the most stable behavior. The deviation from parameter set no. 1 in the first experiment is only sporadically and slightly above the limit of 5%. In the experiments with the torque load of a real application, the rotational speed curve of parameter set no. 1 has the smallest offset. The deviation of the speed between the battery model parameterized with parameter set no. 1 and the real application in the screwing application, as well as in the drilling application, is approx. 20 rpm. Therefore, the percentage deviation between the rotational speeds of parameter set no. 1 and the real application is about 5% and hence is roughly within the limits. Thus, the parameterization method proposed in [26] leads overall to the most accurate results on the test bench.

V. CONCLUSION

Regarding the main questions presented in the paper, the test results lead to the following statements. The power supply has a non-negligible influence on the mechanical parameters of the power tool and must therefore be mapped on the mechanical HiL test bench.

Regarding the effort of simulation of the power source or battery pack, the results show that a mathematical model of the battery is sufficient to simulate the influence of the battery on the mechanical parameters in the early phase of validation. However, the results also show that a minimum amount of experimental data is required for parameterization of the mathematical model used, if sufficient accuracy is needed. Therefore, the parameterization method by Motapon *et al.*, which was used for parameter set no. 1 is a good tradeoff between accuracy and parameterization effort. The results of the model parameterized with parameter set no. 2 show that the thermal parameters R_{th} and t_c are so specific that they have to be extracted experimentally. In addition, the results of the model parameterized with parameter set no. 3 show that a larger experimental fraction does not necessarily lead to a more accurate simulation. In the case of the mathematical model used, the effort of a complete experimental parameterization is therefore unnecessary.

ACKNOWLEDGMENT

The authors of this publication are responsible for its contents.

REFERENCES

[1] H. Haupt, M. Plöger, and J. Bracker, "Hardware-in-the-Loop test of battery management systems," *IFAC Proc. Volumes*, vol. 46, no. 21, pp. 658–664, 2013.
[2] Z. Hui, L. Cheng, and Z. Guojiang, "Design of a versatile test bench for hybrid electric vehicles," in *Proc. IEEE Vehicle Power Propuls. Conf.*, Harbin, China, Sep. 2008, pp. 1–4.
[3] R. M. Schupbach and J. C. Balda, "A versatile laboratory test bench for developing powertrains of electric vehicles," in *Proc. IEEE 56th Veh. Technol. Conf.*, Vancouver, BC, Canada, Oct. 2002, pp. 1666–1670.
[4] L. Gauchia and J. Sanz, "A per-unit Hardware-in-the-Loop simulation of a fuel Cell/Battery hybrid energy system," *IEEE Trans. Ind. Electron.*, vol. 57, no. 4, pp. 1186–1194, Apr. 2010.
[5] R. Morello, R. Di Rienzo, R. Roncella, R. Saletti, and F. Baronti, "Hardware-in-the-Loop platform for assessing battery state estimators in electric vehicles," *IEEE Access*, vol. 6, pp. 68210–68220, 2018.
[6] J. V. Barreras, C. Fleischer, A. E. Christensen, M. Swierczynski, E. Schaltz, S. J. Andreasen, and D. U. Sauer, "An advanced HIL simulation battery model for battery management system testing," *IEEE Trans. Ind. Appl.*, vol. 52, no. 6, pp. 5086–5099, Nov. 2016.
[7] A. Ebner, F. V. Conte, and F. Pirker, "Rapid validation of battery management system with a dymola Hardware-in-the-Loop simulation energy storage test bench," *World Electr. Vehicle J.*, vol. 1, no. 1, pp. 205–207, 2007.
[8] T. Baumhofer, W. Waag, and D. U. Sauer, "Specialized battery emulator for automotive electrical systems," in *Proc. IEEE Vehicle Power Propuls. Conf.*, Lille, France, Sep. 2010, pp. 1–4.
[9] N. Daniil and D. Drury, "Investigation and validation of methods to implement a two-quadrant battery emulator for power Hardware-in-the-Loop simulation," in *Proc. IECON - 42nd Annu. Conf. IEEE Ind. Electron. Soc.*, Florence, Italy, Oct. 2016, pp. 2070–2075.
[10] T. Mesbahi, N. Rizoug, P. Bartholomeus, and P. Le Moigne, "Li-ion battery emulator for electric vehicle applications," in *Proc. IEEE Vehicle Power Propuls. Conf. (VPPC)*, Oct. 2013, pp. 1–8.
[11] D. Worwood, Q. Kellner, M. Wojtala, W. D. Widanage, R. McGlen, D. Greenwood, and J. Marco, "A new approach to the internal thermal management of cylindrical battery cells for automotive applications," *J. Power Sources*, vol. 346, pp. 151–166, Apr. 2017.
[12] C. Ziebert, "A table-driven li-ion battery model for a BMS development platform—Modeling, measurements, implementation and validation," in *Proc. Eur. Battery, Hybrid Fuel Cell Electr. Vehicle Congr.*, 2017, pp. 1–8.
[13] K. Thirugnanam, H. Saini, and P. Kumar, "Mathematical modeling of li-ion battery for charge/discharge rate and capacity fading characteristics using genetic algorithm approach," in *Proc. IEEE Transp. Electrific. Conf. Expo (ITEC)*, Piscataway, NJ, USA, Jun. 2012, pp. 1–6.
[14] A. A.-H. Hussein and I. Batarseh, "An overview of generic battery models," in *Proc. IEEE Power Energy Soc. Gen. Meeting*, Detroit, MI, USA, Jul. 2011, pp. 1–6.
[15] X. Hu, S. Li, and H. Peng, "A comparative study of equivalent circuit models for li-ion batteries," *J. Power Sources*, vol. 198, pp. 359–367, Jan. 2012.
[16] F. Eltoumi, A. Badji, M. Becherif, and H. S. Ramadan, "Experimental identification using equivalent circuit model for lithium-ion battery," *Int. J. Emerg. Electr. Power Syst.*, vol. 19, no. 3, p. 183, 2018.
[17] A. Thanheiser, T. P. Kohler, C. Bertram, and H.-G. Herzog, "Battery emulation considering thermal behavior," in *Proc. IEEE Vehicle Power Propuls. Conf.*, Chicago, IL, USA, Sep. 2011, pp. 1–5.
[18] M. Michalczuk, L. M. Grzesiak, and B. Ufnalski, "Experimental parameter identification of battery-ultracapacitor energy storage system," in *Proc. IEEE 24th Int. Symp. Ind. Electron. (ISIE)*, Buzios, Rio de Janeiro, Brazil, Jun. 2015, pp. 1260–1265.

[19] R. Jackey, M. Saginaw, P. Sanghvi, J. Gazzarri, T. Huria, and M. Ceraolo, "Battery model parameter estimation using a layered technique: An example using a lithium iron phosphate cell," in *Proc. SAE Tech. Paper Ser.*, Apr. 2013, pp. 1–7.
[20] P. B. Praveen Kumar, "Parameter extraction of battery models using multiobjective optimization genetic algorithms," in *14th Int. Power Electron. Motion Control Conf. (PEMC)*, 2010, Ohrid, Republic of Macedonia, 2010, pp. 9–106.
[21] W.-J. Shen and H.-X. Li, "A sensitivity-based group-wise parameter identification algorithm for the electric model of li-ion battery," *IEEE Access*, vol. 5, pp. 4377–4387, 2017.
[22] Z. Wang, J. Ma, and L. Zhang, "Finite element thermal model and simulation for a cylindrical li-ion battery," *IEEE Access*, vol. 5, pp. 15372–15379, 2017.
[23] A. Gaitonde, A. Nimmagadda, and A. Marconnet, "Experimental characterization of thermal conductance across the separator-shell interface in dry cylindrical lithium ion batteries," in *Proc. 16th IEEE Intersociety Conf. Thermal Thermomech. Phenomena Electron. Syst. (ITherm)*, Orlando, FL, USA, May 2017, pp. 1034–1039.
[24] D. H. Jeon and S. M. Baek, "Thermal modeling of cylindrical lithium ion battery during discharge cycle," *Energy Convers. Manage.*, vol. 52, nos. 8–9, pp. 2973–2981, Aug. 2011.
[25] O. Tremblay and L.-A. Dessaint, "Experimental validation of a battery dynamic model for EV applications," *World Electr. Vehicle J.*, vol. 3, no. 2, pp. 289–298, 2009.
[26] S. N. Motapon, A. Lupien-Bedard, L.-A. Dessaint, H. Fortin-Blanchette, and K. Al-Haddad, "A generic electrothermal li-ion battery model for rapid evaluation of cell temperature temporal evolution," *IEEE Trans. Ind. Electron.*, vol. 64, no. 2, pp. 998–1008, Feb. 2017.
[27] *Panasonic UR 18650 RX Li-Ionen Datasheet*, SANYO Energy (U.S.A.) Corporation, Kansas City, MO, USA, 2012.
[28] T. Gwosch, "Antriebsstrangprüfstände zur ableitung Von konstruktionszielgrößen in der produktentwicklung handgehaltener power-tools," Ph.D. dissertation, Inst. Product Eng., Forschungsberichte des IPEK, Karlsruhe, Germany, 2019, vol. 117.

TASSILO SCHRÖDER was born in Rüdesheim, Rheinhessen, Germany, in 1990. He received the B.Sc. degree in mechanical engineering and the M.Sc. degree in mechanical engineering from the Karlsruhe Institute of Technology (KIT), Karlsruhe, Germany, in 2015 and 2017, respectively. Since 2018, he has been a Research Assistant with the IPEK–Institute of Product Engineering, KIT. His research interest includes validation of technical systems in the context of product development, mainly power tools.

THOMAS GWOSCH was born in Donaueschingen, Baden-Württemberg, Germany, in 1989. He received the master's degree in mechanical engineering and the Ph.D. degree in mechanical engineering from the Karlsruhe Institute of Technology (KIT), Karlsruhe, Germany, in 2014 and 2019, respectively. From 2014 to 2019, he worked as a Research Assistant at the IPEK–Institute of Product Engineering, KIT. Since 2019, he has been a Chief Engineer at the IPEK–Institute of Product Engineering, KIT. His research interests include test and validation methods of mechatronic systems with regard to human–machine interaction and powertrain HIL testing.

SVEN MATTHIESEN was born in Gronau, Westfalen, Germany, in 1971. He received the Diploma degree in mechanical engineering and the Ph.D. degree in mechanical engineering from the Karlsruhe Institute of Technology (KIT), Karlsruhe, Germany, in 1997 and 2002, respectively. From 2000 to 2002, he was employed as a Professor at the Technical University in Sofia (Bulgaria) for the subject of Mechanical Design I to III. Then, he worked for HILTI Company, Schaan, Principality of Liechtenstein, until 2010. His last position was the Head of Development in the field of Schraubtechnik (bolt technology). In 2010, he took the offer of a Full Professorship of power tools and machine elements at the IPEK–Institute of Product Engineering, KIT. He is the holder of the chair for power tools and machine elements. Beside his professorship, he is spokesman of the competence field product life cycle at KIT. He is also the Dean of studies for mechatronics and informatics and a board member of the WiGeP, a Scientific Association for product development. His research activities focus on the validation of drive systems, the use of AI approaches in mechatronic systems, and the research into machine elements in the system context. Furthermore, his research includes the fields of human–machine interaction and design cognition. He is a member of the study commission at the faculty of mechanical engineering. His awards and honors include the FAG Foundation's Innovation Award, in 2004, the Martin Hilti Innovation Award, in 2008, and the Wolfgang Beitz Award, in 2008.